Eur. Phys. J. D **3**, 211–216 (1998)

THE EUROPEAN PHYSICAL JOURNAL D

Frequency doubling of a fibre-amplified 1083 nm DBR laser

D.J.E. Knight[1,a], F. Minardi[2,b], P. De Natale[3], and P. Laporta[4]

[1] European Laboratory for Non-Linear Spectroscopy (LENS) and Istituto Nazionale Fisica della Materia (INFM), Largo Enrico Fermi 2, 50125 Firenze, Italy
[2] Dipartimento di Fisica, Università di Pisa, Piazza Torricelli 2, 56126 Pisa, Italy
[3] Istituto Nazionale di Ottica (INO), Largo Enrico Fermi 6, 50125 Firenze, Italy
[4] Istituto Nazionale Fisica della Materia (INFM) and Dipartimento di Fisica, Politecnico di Milano, Piazza Leonardo Da Vinci 32, 20133 Milano, Italy

Received: 25 February 1998 / Revised and Accepted: 28 May 1998

Abstract. A good frequency standard is required at 1083 nm for measurements on the fine structure of helium and of the fine structure constant. Several milliwatts of CW frequency-doubled light offers the prospect of stabilisation to a Doppler-free hyperfine transition in molecular iodine. The 1083 nm emission of an extended-cavity DBR diode laser has been amplified using an ytterbium-doped fibre amplifier, and applied to a type-I phase matched Mg:$LiNbO_3$ crystal in a high-Q fundamental-resonant cavity for frequency doubling. The amplifier gain at 1083 nm under typical operating conditions was 13.8 dB, with a coherent output power up to 63 mW, limited by the maximum signal input power. The doubling cavity Q was $\sim 2 \times 10^7$, and about 70% of the incident power was coupled in. The maximum 2nd-harmonic conversion efficiency exceeded 20% and provided an output power of 3.7 mW for making continuous frequency scans of up to 600 MHz in the green. An optical spectrum analyser at 541.5 nm showed fringes of 4.6 MHz full width half maximum, close to the instrumental width.

PACS. 42.65.Ky Harmonic generation, frequency conversion – 42.72.Ai Infrared sources – 42.72.Bj Visible and ultraviolet sources

1 Introduction

Accurate frequency measurement of the fine-structure energy splittings in helium atom is of interest for determining the fine structure constant, α [1], and for comparison with accurate theoretical calculations. Such measurements were made using DBR diode lasers at 1083 nm, with suitable line-narrowing arrangements [2]. However, at this wavelength, it is difficult to obtain a secondary frequency standard, having an accuracy typical of saturated-absorption signals. A possibility is offered by the spectrum of molecular Cesium $^{133}Cs_2$ [3], but the absorption is weak. An alternative way is to double the frequency and then seek a suitable saturated-absorption dip in the rich I_2 spectrum [4], as at the neighbouring Nd:YAG and similar-laser wavelengths [5, 6]. In the 540 nm spectral region concerned, the I_2 absorptions are strong, but the accompanying hyperfine components have high multiplicity within the Doppler linewidth, and at low pressure can be as narrow as 1 MHz [6] full-width half-maximum (FWHM), although more typically 2-3 MHz [7]. Saturation requires high intensity illumination and the sub-Doppler feature contrast is small, of the order of a few percent [7]. Thus, even when using He-Ne lasers, with their fine tunability and intrinsically narrow linewidth, careful isolation of the laser and sensitive spectroscopic techniques are needed [8]. Contemporaneously with our work, the JILA group demonstrated an alternative route to build new secondary frequency standards based on extremely weak overtone molecular transitions [9].

In our laboratory, we have explored frequency narrowing of the available 1083 nm diode lasers [2], and we decided to pursue frequency doubling of the radiation to 541 nm [10]. Efficient external cavity doubling was previously obtained with CW Nd:YAG lasers, using Mg:$LiNbO_3$ [11,12] and LBO [13] crystals. Doubling 1083 nm radiation generated by DBR lasers is generally less efficient than when using Nd:YAG sources, due to the lower available power. In addition, to achieve frequency narrowing of DBR lasers an external cavity is needed, which couples out only a fraction of the laser power. Therefore, there is a trade-off between output power and narrow emission linewidth in the green. On the other hand, amplification of 1083 nm radiation using Yb-doped fibre amplifiers has been recently demonstrated [14,15].

[a] *Permanent address:* DK Research, 110 Strawberry Vale, Twickenham, TW1 4SH, UK.
e-mail: djek@cix.co.uk
[b] e-mail: minardi@lens.unifi.it

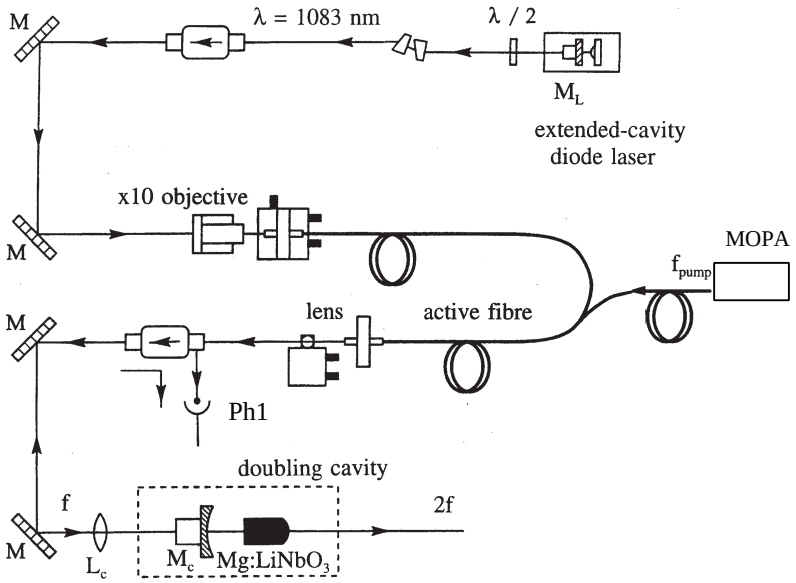

Fig. 1. Schematic diagram of the apparatus. Light from an extended-cavity DBR diode laser is passed through two Faraday-rotation isolators to a high-Q cavity containing a frequency-doubling crystal phase matched at 145(5) °C. An ytterbium-doped fibre (YDF) amplifier is inserted between the two isolators, the second of which separates out the beam reflected from the doubling cavity, that impinges onto photodiode Ph1. The doubling cavity resonance is servoed to the laser frequency by feeding back to the PZT mount of the cavity input mirror M_c. L_c is the cavity mode-matching lens. At the laser M_L is a PZT-mounted 50% transmitting mirror serving as the extended-cavity output mirror.

In this paper we report, for the first time to our knowledge, a detailed characterization for doubling a fibre-amplified 1083 nm source using type I birefringent phase-matching in a semi-monolithic $Mg:LiNbO_3$ crystal mounted in a fundamental-wave enhancement cavity. By this system, we demonstrate the achievement of a 541.5 nm signal at the milliwatt level suitable for saturation absorption in the I_2 spectrum.

2 Experiment

The experimental layout is shown in Figure 1.

The DBR diode laser and its extended-cavity [2] mirror, M_L, was mounted in a 6 mm thick aluminium box. The DBR diode laser was temperature controlled within its can. The extended cavity comprised a 50% reflecting mirror on a piezoelectric transducer (PZT) mount 38 mm from the diode laser. The longitudinal mode spacing of 4 GHz was matched by the laser frequency at current intervals of about 3 mA. The emission passed through a window to a $\lambda/2$ plate followed by a pair of anamorphic prisms adjusted to make the beam circularly shaped before passing through the Faraday-rotation isolator (−30 dB). The beam was then focussed by a 10× microscope objective onto the input facet of the fibre amplifier.

The fibre amplifier was similar to one previously described [14]. A Yb-doped fibre (YDF) about 2.4 m long was pumped by a fibre-coupled semiconductor laser (MOPA, SDL 5762-X8). This laser is composed of an oscillator stage, fed with an injection current of 200 mA, and a semiconductor amplifier stage, with a threshold near 250 mA and a near-linear behaviour thereafter up to the operating current limit of 2.1 A. At this current the output power available at the MOPA output fibre, W_{pump}, was 0.51 W. The pump wavelength was 978 nm, in the high absorption and emission peak of the YDF, and the spectrum was single mode with a bandwidth of a few GHz. A WDM coupler connected, by fusion splicings, the MOPA fibre and the single-mode fibre used for launching 1083 nm radiation to the active YDF. The latter had its output end angle cleaved to minimise in-fibre reflection. Fibre amplified radiation was coupled out with a collimator followed by the second optical isolator (−30 dB). The latter was also used to separate out the light reflected from the doubling cavity and to direct it to a 10 MHz bandwidth InGaAs detector (Ph1 in Fig. 1).

After the isolator the beam was coupled into the frequency-doubling resonant cavity, *via* two alignment mirrors and the mode-matching lens, L_c. This had a focal length of 138 mm, and was positioned 160 mm from the outer surface of the cavity input mirror, M_c. The crystal was a $10 \times 3 \times 3$ mm^3 piece of $Mg:LiNbO_3$ cut for type-I phase matching at a temperature near 150 °C. To form the resonant cavity around the crystal (see Fig. 1) one crystal end was ground convex with radius 25 mm and coated for high reflection (HR) at 1083 nm and antireflection (AR) at 541 nm. The plane face of the crystal was AR coated at both 1083 and 541 nm. The PZT-mounted input mirror M_c with concave face of radius 25 mm and coated for 0.8% transmission at 1083 nm and HR at 541 nm completed the cavity. The measured finesse was about 540 when well

adjusted, indicating a FWHM of about 12 MHz. From the measured finesse, a 240 power amplification factor is inferred.

The crystal was in an oven at the phase matching temperature of 149.6 °C, controlled to about 1 mK. Upper and lower oven plates were also used as electrodes to phase modulate the cavity at 2 MHz to lock its central frequency to that of the laser. The reflected signal was detected and fed back *via* a double-integrating servo to the PZT mount of M_c to hold the cavity centre frequency, indicated by the reflection dip, to the laser frequency. Correction signal was sometimes fed back also to the laser current, to extend the stable frequency feedback range of the main M_c-PZT feedback loop, but under good ambient conditions, this additional control loop turned out to be not strictly necessary. Doubling-cavity servo-loop oscillation showed up clearly, either near 12 kHz, from the first M_c-PZT assembly mechanical resonance, or near 200 kHz if from overdrive of the laser current modulation input. With the configuration chosen for the frequency doubling cavity, the input mirror distance from the crystal proved to be critical, an optimum distance of 2.5 ± 0.5 mm being required. In this condition, radiation coupling on resonance into the cavity was of the order of 80%.

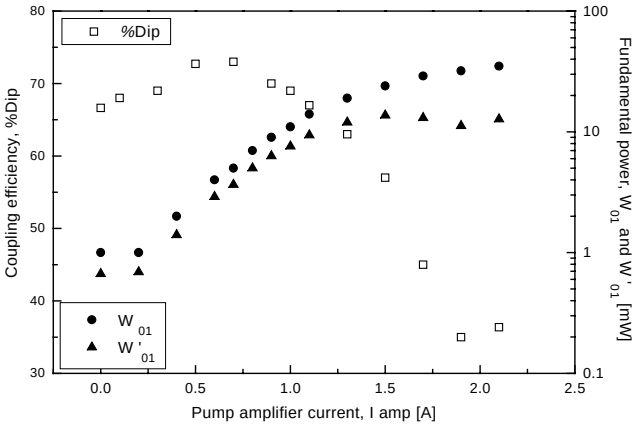

Fig. 2. Frequency doubling cavity input power: incident fundamental power, W_{01}, percent reflection dip, %Dip, and non-reflected power at resonance, $W'_{01} = W_{01} \times$%Dip/100, all against the fibre amplifier pump amplifier current, I_{amp}. The uncertainty in %Dip is ± 3 at each point. The MOPA output power W_{pump} was 0.3 W at $I_{amp} = 1.3$ A and 0.51 W at $I_{amp} = 2.1$ A.

3 Results

3.1 The fibre amplifier

In the set-up used the maximum power from the diode-laser available at the fibre input was about 6 mW, which corresponded to an output power, with fibre-amplifier pump laser off, W_{po}, of 0.8 mW. This shows the total losses, including input coupling, fibre absorption and output coupling to be 8.8 dB, the majority of which was thought to be from the fibre-end coupling, especially the input end, which was rather critical in our set-up. It was necessary to reset the input coupling fibre position, for example, to avoid increased loss of order 30%, on a change of laboratory temperature of about 1 °C. When the highest amplified power is needed, a tapered hemispherical-ended fibre can be used to reduce launching losses to less than 1 dB [16].

With the MOPA pump on, the 1083 nm output power, W_{01}, increased to 19 mW at 1.3 A pump amplifier current ($W_{pump} = 0.3$ W), and to 35 mW at the maximum amplifier current, 2.1 A ($W_{pump} = 0.51$ W). W_{01} was measured after the output isolator and one mirror, and is shown in Figure 2. In this configuration, we obtained up to 63 mW measured after the collimator at the fibre output, which corresponded to 44 mW after isolator and mirror. The amplifier output power proved to be strongly dependent on fusion splicings between YDF and passive fibres, which have different core size and refraction index. Using a longer YDF (about 3 m), our best result was 110 mW after the collimator, with about 16 dB of amplification, defined as the ratio W_{01}/W_{po}. It should be noted that the cavity percent reflection "dip", %Dip, decreased above the "knee" region, see Figure 2, indicating reduced average input coupling of the power seen by the reflection detector. As discussed in [17] and experimentally verified in [14], when increasing the pump power gain saturation at 1083 nm occurs. Thereafter pump power is converted into amplified spontaneous emission (ASE), mainly between 1020 and 1040 nm. For our fibre-amplifier set-up, we expect gain saturation to occur for a MOPA laser power, $W_{pump} \sim 0.3$ W [14], which corresponds to a 1.3 A MOPA current. Therefore, we believe that the cavity dip reduction beyond 1.3 A is due to out-of-band emission in the YDF. In addition, there are uncertainties in the measurement of the dip, ± 3 in %Dip, and time and signal-level variations during the plot recording, so that the $\sim 10\%$ decrease indicated towards low pump current may be spurious. The power not reflected from the doubling cavity is taken to be the power coupled in, W'_{01}, given by the product of the input power W_{01} multiplied by the fractional coupling coefficient (*i.e.* %Dip/100), and is also shown in Figure 2. This can be seen to be approximately flat above 1.3 A MOPA amplifier current.

There was no evidence of any change in the mode or alignment of the amplified beam, related to the pump power W_{pump}. The YDF output power as measured immediately after the fibre end, with a wide aperture detector, and 3.2 m away, with a 1.5×10^{-3} numerical aperture detection, showed the same dependence on the pump power W_{pump}. Also, the mode pattern of the doubling cavity was not affected by W_{pump}, while a change of the amplified beam intensity distribution or alignment would have caused transverse modes of the doubling cavity to appear.

We did not notice any thermal damage of our crystal, even at the highest fundamental power circulating inside the cavity, 3.6 W.

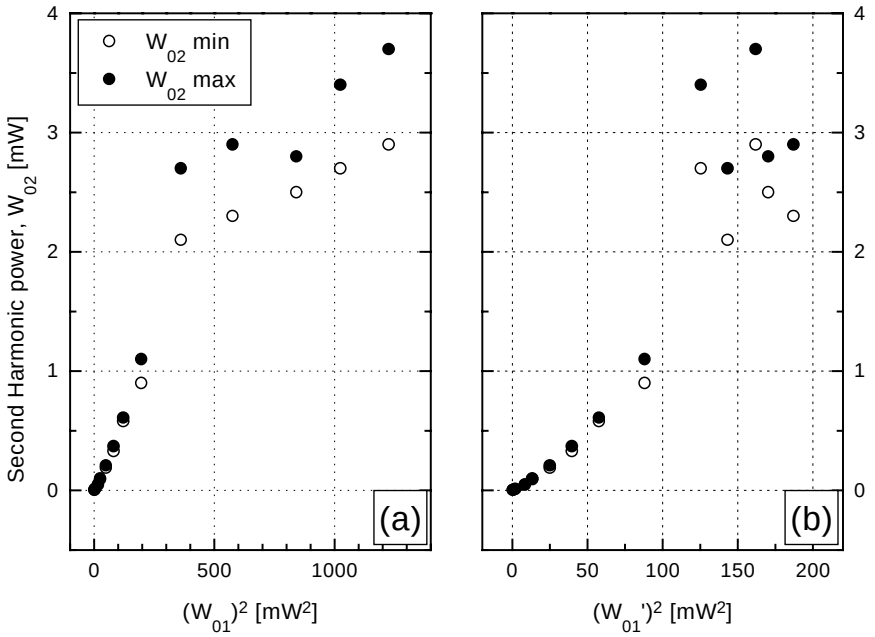

Fig. 3. Second-harmonic output power, W_{02}, against squared, incident fundamental power $(W_{01})^2$ (a), and, to the right, against squared, non-reflected, *i.e.* coupled-in, fundamental power $(W'_{01})^2$ (b). The two-valued points in each case depict the maximum and minimum values occurring in the observed slow "cycling" of the 2nd harmonic output.

3.2 Second harmonic generation

Removing the input mirror, we measured first the single-pass doubling efficiency: 14 nW of harmonic power was generated with 10.8 mW of fundamental radiation. This amounts to a 1.61×10^{-4} W^{-1} non-linear conversion efficiency.

With the doubling cavity servo-locked to the laser and the crystal oven temperature set to optimum temperature, the frequency-doubled output power, typically obtained from a well-aligned cavity, is shown in Figure 3.

Two plots are given: the 2nd harmonic W_{02} is against the incident total power, W_{01}, and against the coupled-in power, W'_{01}. The fundamental power was varied by varying the MOPA power amplifier current, and thus the fibre-amplifier gain, as shown in Figure 2. As the gain is increased, the green output power "cycled" up and down, with a period of the order of 20 s. It can be seen that the cycling amplitude, monotonically increases with amplifier current, and is at a moderate level at the 1.3 A setting chosen for normal use. Interaction of the input 1083 nm power with the crystal temperature servo, or laser-frequency or fibre-temperature drift through étalon fringes arising from reflections in the amplifier fibre could have been responsible. Also, even though the doubling cavity was not resonant for the harmonic radiation, interference occurred between forward-generated green light and green light reflected back off the cavity input mirror M_c: this was thought to cause a sharp temperature-tuning peak, *via* a temperature-dependent phase shift at the input mirror and/or at the crystal face. In fact, the temperature-tuning curve of the harmonic power was much narrower for cavity doubling than for single-pass.

The frequency-doubled power levels achieved were about 2-2.5 mW at 1.3 A, and 2.7-3.5 mW at 2.1 A, which means, respectively, 17-21% and 23-29% of the power coupled into the cavity W'_{01}. The cavity input coupling was typically 63% at 1.3 A and 36% at 2.1 A.

We reached a non-linear doubling efficiency of 1.7×10^{-4} W^{-1}. This value is about one order of magnitude lower than the maximum doubling efficiency expected at 1.06 μm: 2.1×10^{-4} W^{-1} [18].

The plots of Figure 3 show the square-law behaviour expected, up to the amplifier saturation region. The scatter at the top of the corrected curve results mainly from measurement uncertainties, and its lying a little above the square law line may result from under-estimating the fundamental power coupled in, in the presence of out-of-band fluorescence. The latter, in fact, does not couple into the cavity, thus decreasing the measured coupling efficiency. In addition, its shorter wavelength contribution to the total power is over-estimated by the InGaAs photodiode Ph1. Also, fluctuations in the spectrum of the out-of-band fluorescence may be the origin of the scatter of the estimated coupled-in power (see Fig. 3b). Concerning the optical alignment of the doubling cavity, the highest input coupling dip observed was (84 ± 3)%, with the cavity modulation and amplifier off, compared with a theoretical value of about 86%, indicating that the coupling efficiency is well optimised. Cavity phase/frequency modulation, typically of 400 mV corresponding to about 4.8 MHz peak-peak, was needed for the servo to suppress room acoustic noise, and this reduced the dip to about 70%. As already pointed out, increasing MOPA amplifier current above 1.3 A further reduced the dip to about 63% and down to 36%

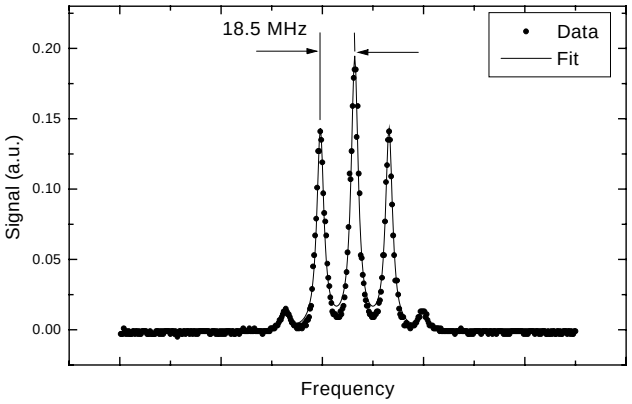

Fig. 4. Typical green-light fringes seen on a 300 MHz free spectral range Fabry-Perot spectrum analyser after passing the electro-optic modulator. The modulation frequency is 18.5 MHz and modulation index 1.3. The FWHM of peak and sidebands is ~ 4.6 MHz, mainly from the instrumental width. The fitting line is given by the sum of 5 Airy's functions.

at 2.1 A (see Fig. 2). The highest coupling observed at 1.3 A was $(69 \pm 3)\%$.

3.3 Quality of 2nd harmonic output radiation at 541.5 nm

The green generated radiation was passed through a collimating lens and then through an electro-optic modulator with input and output focusing lenses. The modulated light was spectrally examined using a 300 MHz free spectral range Fabry-Perot spectrum analyser. A typical spectrum of the 541.5 nm output with 18.5 MHz modulation sidebands is shown in Figure 4. The modulation sidebands are well separated and the width of the peaks is 4.6 MHz, scaling from the sideband spacing. The modulation index is 1.3. Decreasing the modulation frequency to 10.1 MHz and the modulation index to 0.7, the output signal still had well-resolved sideband peaks. This likewise indicated a narrow doubled-light spectrum. Data of Figure 4 and of the 10.1 MHz spectrum were fitted with multiple Airy peaks: the resulting FWHM is (4.55 ± 0.15) MHz, corresponding to a finesse of 65 ± 2. Taking the value given in the specifications of the Fabry-Perot (Burleigh mod. 216-B), $F = 95$ at our wavelength, as an upper limit for the finesse, we obtain a ~ 1.4 MHz upper limit for the FWHM of the second-harmonic spectrum, assuming that the latter is Lorentzian shaped. Moreover, we have tested the Fabry-Perot cavity with a frequency-doubled Nd-YAG laser (Lightwave mod. A 142), whose green emission linewidth is in the 10 kHz range, and the measured finesse agrees with the specifications.

The Fabry-Perot is a factor 5 more sensitive than the doubling cavity as a discriminator for the amplified laser signal width, and may be used to check the coupling optimisation of harmonic power into the sidebands. The scans were done by driving the M_L PZT in the laser extended cavity (see Fig. 1).

4 Discussion and conclusions

The 2nd-harmonic radiation generated with the aid of the amplifier reached power levels suitable for saturating the desired hyperfine transitions in molecular iodine. However, there were amplitude fluctuations in the fundamental at the doubling cavity input, mainly at a few Hz or lower, which impeded the cavity locking process by affecting the loop gain, and also fed through into the green light. These might be attributable to reflection fringes in the active fibre, which could be reduced by care in arranging the end facets. Feedback to the laser itself was a concern, which can be solved by an additional isolator before the fibre amplifier, since this amplifies in both directions. Its low gain at the laser frequency probably helped in this respect. Two 5-mm diameter stops were also placed in the beam reflected from the cavity, before the isolator, at 1.5 m, and again before the fibre output collimator. Apart from fringing effects, the chief cause of a.m. noise in the green output was from unsuppressed vibration and acoustic disturbance of the doubling cavity length. The optical pathlength of the doubling cavity corresponded to 25 mm in air, and in view of the high Q, 2×10^7, a change of 1 part in 10^7 would have a strong effect: this is only 2.5 nm, easily achieved by touching the wires connected to our teflon-mounted oven. Much of the noise spectrum was around 20-30 Hz.

The doubling cavity passive stability was estimated in previous work [10], by reversing the locking loop configuration, *i.e.* by locking the laser to the doubling cavity. Using an iodine line as a discriminator, we found that the frequency fluctuations in the green, corresponding to length fluctuations of the doubling cavity, were of the order of 100 MHz, 4 parts in 10^7. This can be improved by a more rigid crystal oven assembly. A bonus would be the reduced modulation of the doubling cavity needed to retain lock, resulting in a higher doubling efficiency.

There was no evidence, when all was running well, of spectral broadening of the laser emission by the amplifier, only of out-of-band emission. However, the linewidth of the extended-cavity diode laser may be marginal for interrogating the iodine hyperfine lines at low pressure, reported at 1 MHz FWHM [6]. The 38-mm extended cavity length is much less than that of a typical He-Ne laser, used in references [7] and [8], giving a smaller stored energy and Q, and the diode laser, being of small dimensions, is also prone to high-frequency noise. The diode-pumped Nd:YAG laser used in references [5] and [6] is unusually narrow in its spectrum, and is optically-pumped over a much larger volume than that of the active region of a diode laser. Our extended cavity was about 1/3 the length of that in reference [2], for which a single-laser heterodyne spectral width of (170 ± 50) kHz was given, for a 60%-reflecting mirror. We plan to improve our set-up by further narrowing the DBR laser linewidth with a stronger optical feedback. A different, more efficient amplifier scheme [15] will compensate for the lower power output. With such a scheme, we plan to get about 0.5 W of 1083 nm amplified radiation, which makes possible a parallel reduction of the doubling cavity finesse. The latter characteristics, together with a more rigid cavity construction, will assure

a much improved stability of the lock and reduced amplitude noise. A further simplification of the set-up can come from the use of quasi-phase-matching second harmonic generation in periodically poled crystals, such as $LiNbO_3$ (PPLN) and $KTiOPO_4$. Indeed, single-pass doubling efficiencies of 4.6% at 946 nm and 1% at 1064 nm have been demonstrated in a bulk PPLN [19,20] while up to 20% SHG efficiency was obtained in a PPLN waveguide at 843 nm [21]. With such possibilities we continue actively working to use doubled green light to saturate iodine transitions.

We are grateful to Prof. D.C. Hanna and Dr. R. Paschotta for useful suggestions and for kindly supplying the Yb-doped fibre. We wish to thank also Dr. A. Arie for designing the doubling cavity, Dr. M. Prevedelli for his valuable help with the stabilisation electronics and Prof. M. Inguscio for his support and continuous encouragement. This work was performed in the frame of EC contract TMR ERB FMGE CT950017.

References

1. M. Inguscio, G. Giusfredi, F.S. Pavone, M. Prevedelli, Phys. Scripta T **70**, 42-47 (1997).
2. M. Prevedelli, P. Cancio, G. Giusfredi, F.S. Pavone, M. Inguscio, Optics Commun. **125**, 231-236 (1996).
3. A. Arie, P. Cancio Pastor, F.S. Pavone, M. Inguscio, Optics Commun. **117**, 78-82 (1995).
4. S. Gerstenkorn, P. Luc, *Atlas du spectre d'absorption de la molecule d'iode* (Éditions du CNRS, Paris, 1978).
5. A. Arie, S. Schiller, E.K. Gustafson, R.L. Byer, Optics Lett. **17**, 1204-1206 (1992).
6. P.A. Jungner, S. Swartz, M. Eickhoff, J. Ye, J.L. Hall, S. Waltman, IEEE Trans. Instrum. Meas. **44**, 151-154 (1995); M. Eickhoff, J.L. Hall, *ibid.* 155-158.
7. W.R.C. Rowley, private communication.
8. T. Lin, Y.-W. Liu, W.-Y. Cheng, J.-T. Shy, B.-R. Jih, K.-L. Ko, Optics Commun. **107**, 389-394 (1994).
9. Jun Ye, Long-Sheng Ma, J.L. Hall, J. Opt. Soc. Am. B **15**, 6-15 (1998).
10. F. Minardi, D.J.E. Knight, A. Arie, F.S. Pavone, F. Venturini, M. Inguscio, in *Laser Spectroscopy XIII*, edited by Zhi-jiang Wang, Zhi-ming Zhang, Yu-zhu Wang, (World Scientific, Singapore 1998), pp. 469-471.
11. W.J. Kozlovsky, C.D. Nabors, R.L. Byer, IEEE J. Quantum Electron. **QE-24**, 913-919 (1988).
12. K. Schneider, S. Schiller, J. Mlynek, M. Bode, I. Freitag, Optics Lett. **21**, 1999-2001 (1996).
13. S.T. Yang, C.C. Pohalsky, E.K. Gustafson, R.L. Byer, R.S. Feigelson, R.J. Raymakers, R.K. Route, Optics Lett. **16**, 1493-1495 (1991).
14. R. Paschotta, D.C. Hanna, P. De Natale, G. Modugno, M. Inguscio, P. Laporta, Optics Commun. **136**, 243-246 (1997).
15. S.V. Chernikov, J.R. Taylor, N.S. Platonov, V.P. Gapontsev, P.J. Nacher, G. Tastevin, M. Leduc, M.J. Barlow, Electron. Lett. **33**, 787-789 (1997).
16. Technical Staff of CSELT, *Fiber Optic Communication Handbook*, 2nd edition (McGraw-Hill, New York 1990), pp. 482-490.
17. R. Paschotta, J. Nilsson, A.C. Tropper, D.C. Hanna, IEEE J. Quant. Electron. **QE-33**, 1049-1056 (1997).
18. V.G. Dimitriev, G.G. Gurzadyan, D.N. Nikogosyan, *Handbook of Non-linear Optical Crystals* (Springer-Verlag, Berlin, 1991).
19. V. Pruneri, R. Koch, P.G. Kazansky, W.A. Clarkson, P. St.J. Russel, D. Hanna, Optics Lett. **20**, 2375-2377 (1995).
20. A. Arie, G. Rosenman, A. Korenfeld, A. Skliar, M. Oron, M. Katz, D. Eger, Optics Lett. **23**, 28-30 (1998).
21. J. Webjorn, S. Siala, D.W. Nam, R.G. Waarts, R. J. Lang, IEEE J. Quantum Electron. **QE-33**, 1673-1686 (1997).